Single Cell Real-Time miRNAs Sensing Based on Nanomotors

Berta Esteban-Fernández de Ávila,[†] Aída Martín,[†,‡] Fernando Soto,[†] Miguel Angel Lopez-Ramirez,[†] Susana Campuzano,[§] Gersson Manuel Vásquez-Machado, Weiwei Gao,[†] Liangfang Zhang,[*,†] and Joseph Wang[*,†]

[†]Department of Nanoengineering, University of California, San Diego, La Jolla, California 92093, United States, [‡]Department of Analytical Chemistry, University of Alcalá de Henares, E-28871 Madrid, Spain, and [§]Department of Analytical Chemistry, Complutense University of Madrid, E-28040 Madrid, Spain

ABSTRACT A nanomotor-based strategy for rapid single-step intracellular biosensing of a target miRNA, expressed in intact cancer cells, at the single cell level is described. The new concept relies on the use of ultrasound (US) propelled dye-labeled single-stranded DNA (ssDNA)/graphene-oxide (GO) coated gold nanowires (AuNWs) capable of penetrating intact cancer cells. Once the nanomotor is internalized into the cell, the quenched fluorescence signal (produced by the $\pi-\pi$ interaction between GO and a dye-labeled ssDNA) is recovered due to the displacement of the dye-ssDNA probe from the motor GO-quenching surface upon binding with the target miRNA-21, leading to an attractive intracellular "OFF-ON" fluorescence switching. The faster internalization process of the US-powered nanomotors and their rapid movement into the cells increase the likelihood of probe–target contacts, leading to a highly efficient and rapid hybridization. The ability of the nanomotor-based method to screen cancer cells based on the endogenous content of the target miRNA has been demonstrated by measuring the fluorescence signal in two types of cancer cells (MCF-7 and HeLa) with significantly different miRNA-21 expression levels. This single-step, motor-based miRNAs sensing approach enables rapid "on the move" specific detection of the target miRNA-21, even in single cells with an extremely low endogenous miRNA-21 content, allowing precise and real-time monitoring of intracellular miRNA expression.

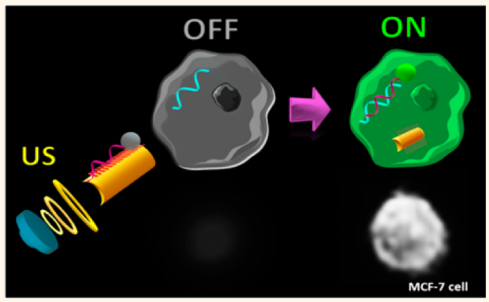

KEYWORDS: miRNAs · real-time biosensing · single intact cancer cells · nanomotors · graphene oxide · ultrasound

MicroRNAs (miRNAs) are small (18–25 nucleotides), endogenous, single-stranded non-protein-coding RNAs, encoded in the genomes of plants, animals, and some virus species. These miRNAs play a major role in regulating important biological processes through the modulation of gene expression, including early development, cell differentiation, hematopoiesis and proliferation.[1] Moreover, abnormal expression of specific miRNAs is associated with many diseases, ranging from cancer to diabetes.[2] miRNAs have thus been regarded as biomarker candidates in disease diagnosis and therapy. Accordingly, the development of effective miRNA detection methods is of considerable clinical importance.[3]

Different methods for detecting miRNA have been described and reviewed recently.[4–6] These include Northern blotting,[7] real-time quantitative RT-q-PCR,[8,9] microarrays,[10,11] and electrochemical, fluorescence or electrochemiluminescence sensors.[5,12–14] Despite major advances made toward sensitive miRNA detection, only few of these methods have demonstrated the possibility to perform real-time miRNA sensing in human serum[15] or miRNA detection in intact cells,[2,16] which are of major clinical significance. Such intracellular detection methods require long incubation times (~14 h) at 37 °C along with a high cell density suspension (~6×10^4 cells) to detect the target miRNA expression. These methods also do not allow single-cell analysis, so important information is lost when thousands of cells are profiled simultaneously, including cell identity and heterogeneity across cell populations. Accordingly, there are urgent needs for methods that can achieve miRNA expression analysis of at single-cell resolution.

In this paper, we describe the use of novel nanomotors for rapid and sensitive intracellular miRNA detection. The feasibility of the new nanomotor approach was demonstrated for miRNA-21 detection, which is found to be overexpressed in 80% of tumor

* Address correspondence to josephwang@ucsd.edu, zhang@ucsd.edu.

Received for review May 8, 2015 and accepted June 2, 2015.

Published online June 02, 2015
10.1021/acsnano.5b02807

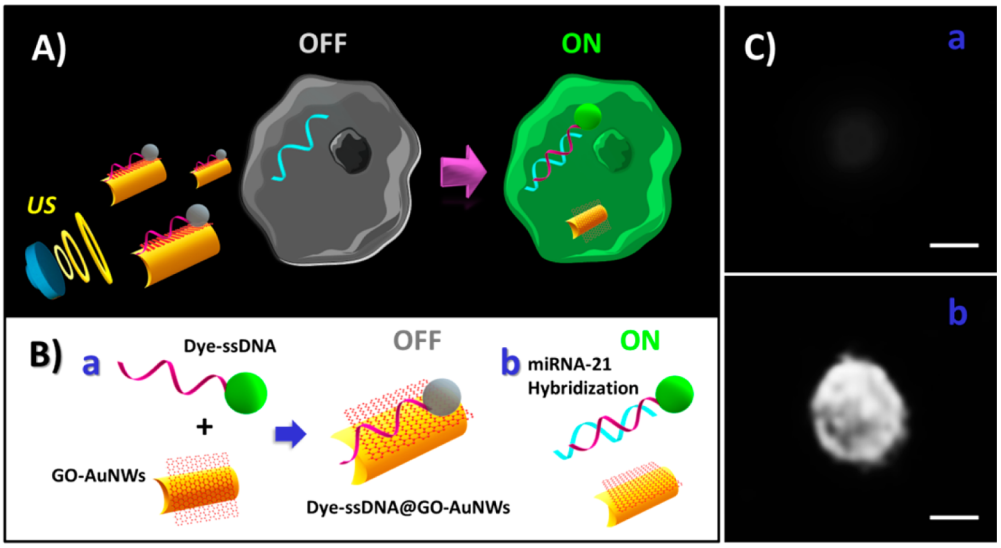

Figure 1. Intracellular detection of miRNAs by US-propelled ssDNA@GO-functionalized gold nanomotors. Schematic illustrations of (A) the "OFF-ON" fluorescent switching system for the specific detection of miRNA-21 in intact cancer cells, and (B) steps involved: (a) immobilization of the dye-ssDNA on the GO-functionalized AuNWs and quenching of the dye fluorescence, and (b) fluorescence recovery due to release of the dye-ssDNA from the motor GO-quenching surface upon hybridization with the target miRNA. (C) Fluorescence images of a MCF-7 cell (a) before and (b) after 20 min incubation with the ssDNA@GO-modified AuNWs under an US field (with 6 V and 2.66 MHz). Scale bar, 10 μm.

samples.[17] The motor-based miRNA sensing strategy combines the advantages of using graphene oxide (GO) for fluorescence-quenching biosensing of nucleic acids,[18,19] with the ability of ultrasound (US)-propelled nanowire (NW) motors to be internalized into the cells,[20] and accelerate the intracellular hybridization process toward rapid "on the move" miRNAs detection with single-cell resolution.

The field of nano/micromachines is expected to lead the development of innovative biosensing strategies.[21−25] Besides operating in previously inaccessible microscale biological environments, nanomotors can lead to fundamentally new sensing approaches. The continuous movement of receptor-functionalized nanomotors has been shown to increase the likelihood of target-receptor contacts and thus to greatly increase the sensitivity while reducing largely the assay time of bioaffinity assays.[25] With increased sophistication and functionalization, future nanomachines are expected to perform more demanding analytical tasks.

Major advances in the nanomotor field[23,26−29] have led to the growing use of nanomotors in diverse environmental,[30−33] biomedical,[34−36] and sensing[21,37−40] applications. Recent efforts have led to the development of fuel-free US-powered motors, which have attracted considerable interest due to their potential biomedical possibilities, including microsurgery,[41] isolation of biological targets,[42] drug delivery,[42,43] and movement within living cells.[20]

Carbon-based nanomaterials, including carbon nanotubes (CNTs),[44] GO,[2] and carbon nanoparticles,[45] have been used as common fluorescence quenchers. In particular, GO has been suggested to be a very efficient quencher due to its high surface area and two-dimensional structure.[46,47] These characteristics allow the adsorption of fluorophore-labeled probes through π-stacking interactions between the nucleotide bases and the carbon nanomaterial, leading to quenching of the fluorescence due to the fluorescence resonance energy transfer (FRET) effect through fluorophore (photodonor)/quencher (photoacceptor) system.

The nanomotor-based fluorescent sensing strategy, described in the present work, allows for the first time real-time monitoring of a target miRNA at single-cell level. For such purpose, ssDNA@GO-modified AuNWs were prepared, by covalent immobilization of a GO sheet onto cysteamine-modified AuNWs through EDC/NHS chemistry, and applied to directly monitor the expression of a target miRNA in intact cancer cells. As illustrated in Figure 1, the nanomotor-based miRNA fluorescence "ON" sensing approach relies on the fast recovery of the quenched fluorescence of a dye-labeled specific single-stranded DNA (ssDNA) probe due its preferential binding with the target miRNA-21 compared to the GO surface (responsible for the quenching). The applicability of the approach is illustrated in the following sections for miRNA-21 detection in both a cell-free system and in intact cancer cells with different expression levels of the target miRNA. The new nanomotor-based real-time miRNA monitoring strategy offers a dramatic acceleration of the hybridization time, to enable fast, ultrasensitive and specific detection of the target miRNA-21 in intact individual cells at room temperature within few minutes compared to several hours and large number of cells required by existing miRNA detection methods. The new strategy thus holds considerable promise for

in situ miRNA expression analysis at single-cell resolution for basic research and clinical diagnostics.

RESULTS AND DISCUSSION

Fabrication of ssDNA@GO-Functionalized Gold Nanomotors. The new nanomotor strategy offers a rapid and specific intracellular detection of miRNA-21. Figure 1A illustrates the "OFF-ON" fluorescence switching approach developed for monitoring the expression of a target miRNA in intact cancer cells using US-propelled ssDNA@GO-functionalized gold nanomotors. The GO-functionalized AuNWs serve as ultrasound-propelled vehicles, transporting the ssDNA capture probe into the cell. Upon entering the cell, the ssDNA probe, attached to the GO-functionalized AuNWs, binds to a specific target miRNA through complementary base-pairing, releasing it from the motor and turning the fluorescence "ON". The template electrosynthesis of AuNWs and their covalent modification with GO are detailed in the Experimental Section. These nanomotors constituted promising platforms for carrying the fluorescein amidine (FAM)-labeled ssDNA probe and internalizing it into intact cells within a few seconds. Different features of GO are exploited in this *in situ* sensing nanovehicles. First, the inherent structure of GO provides a suitable scaffold for the spontaneous adsorption of ssDNA onto its surface by noncovalent π-stacking interactions between the ring structures of the nucleotide bases in the ssDNA and the GO sheet.[48] Experimental results indicate that this mechanism occurs within 2−3 min, which is faster than using single-walled CNTs due to the availability of a high planar surface.[49] Second, owing to the optical and photophysical features of GO, and due to the close proximity of the FAM-ssDNA to graphene, GO acts as an effective quencher for the FAM dye fluorophore, rapidly switching its fluorescence "OFF" (Figure 1B(a)). The presence of the target miRNA leads to its rapid hybridization to the dye-labeled DNA and to release the resulting RNA−DNA hybrid duplex from the motor, due to the weaker interaction between the DNA−miRNA duplex and GO.[50,51] This results in rapid recovery of the dye fluorescence due to the remoteness of the GO quencher, and in a readily detectable signal (Figure 1B(b)). The images of Figure 1C illustrate the "OFF-ON" fluorescence switching inside one single MCF-7 cell (with target miRNA-21 overexpression) using US-propelled modified nanomotors following a 20 min incubation (a *vs* b). These images clearly demonstrate the feasibility of the new method to detect the target miRNA in a single and intact breast cancer cell, as will be described in detail below.

Scanning electron microscopy (SEM) images were carried out to examine the structural morphology of the GO-AuNWs. Figure 2A shows the SEM images of an unmodified AuNW with 4 μm length and a diameter of 200 nm (see inset). The later reflects the pore size of the anodic aluminum oxide membrane template used in the fabrication process. The solid smooth surface of the NW demonstrates the gold morphology. Furthermore, the resulting NWs present a concave end, essential for the acoustic propulsion mechanism, as motion is achieved due to a pressure gradient generated by the scattering of US waves at such concave end.[42,52,53] The AuNWs were modified *via* the self-assembly of the cysteamine bifunctional agent on the gold surface,[54] to bond with GO *via* EDC/NHS coupling of the cysteamine amine group and the carboxylic acid groups of GO. The SEM images of the modified GO-AuNW (Figure 2B) show the thin and folded GO layers covering the entire surface of the AuNW, demonstrating the successful modification of the nanomotor with GO.

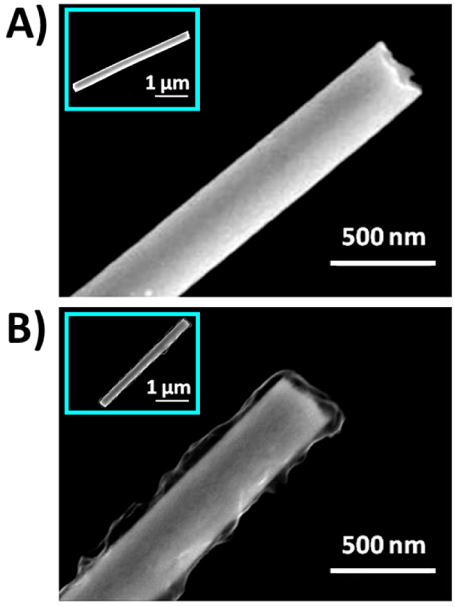

Figure 2. SEM images of (A) unmodified AuNW and (B) GO modified AuNW. Insets: whole AuNW and GO-AuNW structures. AuNW length, 4 μm.

Detection of miRNA-21: *In Vitro* Studies. Prior to studying the intracellular miRNA-21 detection, we evaluated the fluorescence quenching ability of the GO coating by examining the change of the fluorescence signal of the FAM-labeled ssDNA@GO-functionalized AuNWs in the absence and presence of the synthetic miRNA-21 target. FAM-ssDNA exhibited a strong fluorescence signal, characteristic of the FAM dye at λ_{em} 520 nm (λ_{ex} 495 nm). When the GO-AuNWs were incubated with FAM-ssDNA, the FRET effect provoked that the photons absorbed by the FAM dye were transferred to the GO acceptor with high efficiency, thus decreasing the fluorescence down to the corresponding background value. Such behavior reflects the strong and fast quenching effect of GO on the fluorescence of FAM-ssDNA.[55]

To demonstrate the feasibility of the nanomotor approach toward miRNA detection, we compared the fluorescence signals observed after incubating the

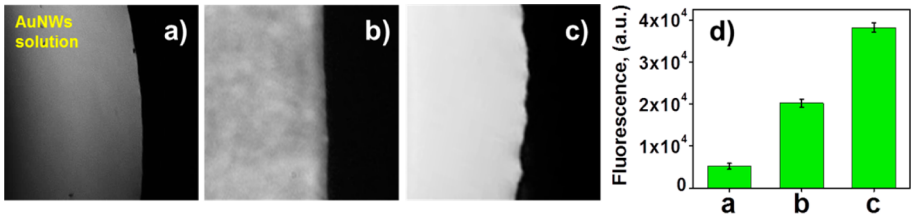

Figure 3. *In vitro* **assay. Fluorescence recovery caused by the hybridization process between the ssDNA capture probe immobilized onto the GO-AuNWs and the synthetic target miRNA-21 at 100 nM. Fluorescence images of the ssDNA@GO-modified AuNWs solution taken after 5 min incubation with the target miRNA-21 using (a) static conditions and applying US at (b) 6 V and (c) 9 V. In black, background signals. (d) Fluorescence signals corresponding to (a), (b) and (c) images (background subtracted). Error bars estimated as a triple of the standard deviation (*n* = 3).**

ssDNA@GO-modified AuNWs with 100 nM synthetic target miRNA-21 for 5 min under static conditions or upon propelling the wires at various speeds. As illustrated in Figure 3a,d (a, green bar), even under static conditions, the fluorescence signal is five times higher than the one obtained in the absence of the target miRNA (5000 au *vs* 1000 au, unshown value). This reflects the extremely high quenching efficiency of GO (that leads to high signal-to-background ratios) and the hybridization of the target miRNA with the ssDNA (attached to the GO-AuNWs). No FAM fluorescence signal was observed after incubating the target miRNA (100 nM) with the unmodified AuNWs (without GO) for 10 min under static conditions, reflecting the crucial role of the FAM-ssDNA/GO coating. Figure 3b,c depicts the fluorescence images obtained in the presence of 100 nM miRNA after applying US voltages of 6 and 9 V, respectively. The corresponding fluorescence values of 20 000 and 38 000 au for 6 and 9 V, respectively (Figure 3d (b and c, green bars)), demonstrate a dramatic improvement in the hybridization efficiency due to the motor movement, as compared to the 5000 au observed under static conditions. The fast motor movement thus accelerates the transport of the target miRNA to the surface DNA probe, resulting in a much more efficient duplex formation, as expected for "on the move" hybridization processes.[37] As a result, the fluorescence "ON" hybridization signal is directly related to the applied US voltage and corresponding motor speed (Figure 3d). It is important to note also that applying US at 9 V resulted in ~60% recovery of the fluorescence intensity within 5 min, compared to the 30 min needed for recovering half of the fluorescence under static conditions[18] or to 60 min for 86% recovery using a different miRNAs fluorescent quenching detection scheme.[50] Overall, the data of Figure 3 thus demonstrate the distinct speed and efficiency advantages of the new nanomotor miRNA detection method.

Furthermore, the selectivity of this new nanomotor approach was evaluated by comparing the fluorescence signal for the miRNA-21 target with the signal obtained from a synthetic 1-mismatched (1-m) sequence, after applying US at 9 V during 5 min. The 1-m sequence leads to an 80% of the fluorescence signal given by the fully complementary target miRNA-21. These data demonstrate a satisfactory discrimination, in agreement with previous reports,[56] considering that the 1-m tested is located in the center of the sequence (see underlined base in sequence 1-m in Supporting Information Table S1).

Detection of Endogenous miRNA-21: Intracellular Studies. The practical utility of this nanomotor methodology was further demonstrated by detecting in real time the target miRNA expression inside intact cancer cells. To perform these studies, we employed a well-characterized estrogen-receptor-positive metastatic breast-cancer cell line (MCF-7). This is a useful cell-based model of breast-cancer cells, with a very high endogenous content of miRNA-21.[57] As control experiments, we switched to the HeLa cells (human epithelial cervix carcinoma cells) as they have an extremely low endogenous level of the mature miRNA-21.[58,59]

Figure 4 shows the actual time-lapse images (taken from Supporting Information Video 1) illustrating the internalization process by US propulsion of one ssDNA@GO-functionalized AuNWs (indicated by a red circle) into a single MCF-7 cell, with additional modified AuNWs inside the cell and others stuck on its membrane. These results demonstrate that the US-propelled ssDNA@GO-functionalized AuNWs interact dynamically with intact cancer cells, similar to the reported internalization of bare AuNWs.[20] The latter study also reported that some AuNW motors stick to the cell membrane. The functionalized AuNWs can be internalized in a few seconds, remained acoustically active and undergo both directional and spinning motion inside the cells (see SI Video 2 and Video 3 in Supporting Information). These results are particularly relevant since the early study which reported the internalization of gold rods required prolonged incubation times (~24 h).[20] The faster internalization can be attributed to the hydrophilic character of GO, that possesses oxygen-contained functional groups (hydroxyl, carboxyl, ester). This character results in the high stability of the GO in aqueous solutions and minimization of the *in vivo* aggregation of the GO sheets, and facilitates its internalization into the cells and its following degradation.[60]

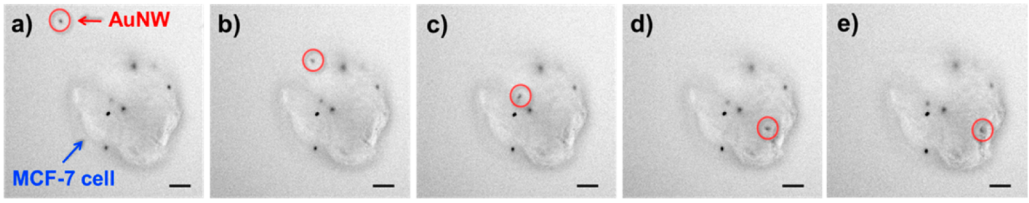

Figure 4. US-powered functionalized AuNWs in the presence of MCF-7 cells. (a−e) Actual time-lapse images taken from Supporting Information Video 1 (4 s intervals) illustrating the internalization process of one modified AuNWs (red circle) into a representative single MCF-7 cell (blue arrow) with other AuNWs already internalized while others stuck on the membrane. US field, 6 V and 2.66 MHz. Scale bar, 10 μm.

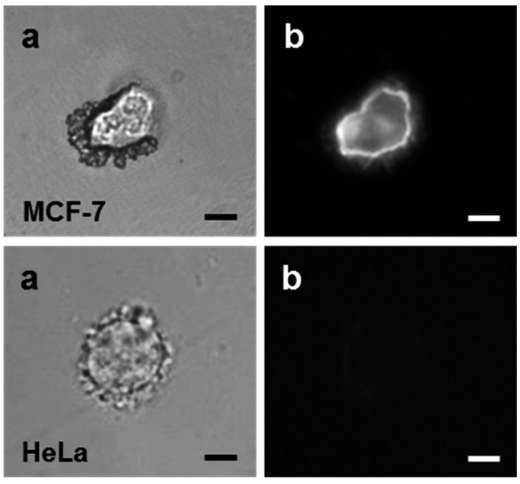

Figure 5. Specific detection of miRNA-21 in different cell lines. (a) Optical and (b) fluorescence images of representative single MCF-7 and HeLa cells after 10 min incubation with the ssDNA@GO-modified AuNWs under an US field (6 V and 2.66 MHz). Scale bar, 10 μm.

To examine the feasibility of the motor-based single cell sensing approach, we compared the fluorescence signals obtained after 10 min incubation with the ssDNA@GO-modified AuNWs in two cancerous cell lines with significantly different endogenous level of the target miRNA-21: MCF-7 and HeLa cells (Figure 5). Once demonstrated, the internalization process of the modified nanomotors into both types of cells (see Supporting Information Videos 1−3), the fluorescence images of both cell lines, obtained under similar experimental conditions and using a similar amount of cells ($\sim 1.5 \times 10^2$ cells), were compared. For clarity, toward demonstrating the single-cell resolution of the nanomotor approach, Figure 5 shows the fluorescence images of single representative MCF-7 (a) and HeLa (b) cells. The intracellular delivered ssDNA@GO-modified AuNWs resulted in the recovery of the FAM fluorescence signal. The different intensity for these cancer cell lines reflects the different degrees of miRNA-21 expression levels. The fluorescence intensity observed inside MCF-7 cells is 44 times higher than that found inside HeLa cells (3750 *vs* 85 au). These results are consistent with previous findings[61] and confirm the higher expression of the target miRNA-21 in the MCF-7 compared to HeLa cells. As shown in Supporting Information Figure 2a, the nanomotor-based miRNA sensing was robust enough to minimize nonspecific fluorescence signal, thus, yielding sensitive and quantifiable response to the target miRNA with low basal fluorescence even in intact cancer cells. These results also demonstrate the screening potential of the single-cell strategy, depending on the endogenous expression level of the target miRNA in the target cells, along with the high sensitivity of the nanomotor method, and its ability to detect the target miRNA in a single cell, including cells with an extremely low endogenous miRNA content such as HeLa (85 au compared to 20 au, in the absence of target miRNA-21). The latter is commonly undetectable for other PCR-amplification free miRNAs biosensing methodologies.[2,56] Note also that the recovery of fluorescence inside a single MCF-7 cell is achieved within 5 min incubation with ssDNA@GO-modified AuNWs (2150 au) under an US field at 6 V and 2.66 MHz (see Figure 6B(b) and corresponding green bar in Figure 6B(e)).

To improve the sensing methodology based on the hybridization-induced fluorescence recovery inside the cells, the influence of the US exposure time and the applied voltage was further examined. Figure 6A shows fluorescence images of the MCF-7 cells after 10 min incubation with the ssDNA@GO-modified AuNWs using static conditions (Figure 6A(a)), and under US field (2.66 MHz) at different voltages (3−9 V, Figure 6A-(b−d, respectively)). These images show that the fluorescence inside the cells increases upon raising the applied amplitude voltage values; at the maximum voltage (9 V), the fluorescence intensity is 17 times higher than under static conditions (Figure 6A(e)). These results demonstrate again the major role of the nanomotor propulsion in facilitating the internalization into the cells and the hybridization efficiency with the target miRNA at room temperature. The miRNA fluorescence signal depends linearly on the US voltage amplitude and the propulsion time, as illustrated in Figure 6A(e), B(e), respectively, resulting in stable fluorescence intensities after 20 min incubation with the modified nanomotors under a 6 V and 2.66 MHz US field (see Supporting Information Figure 2g).

These results demonstrated that the nanomotor detection strategy has the potential to monitor the dynamic changes of miRNA expression in intact single cancer cells, quantitatively, conveniently, in real time

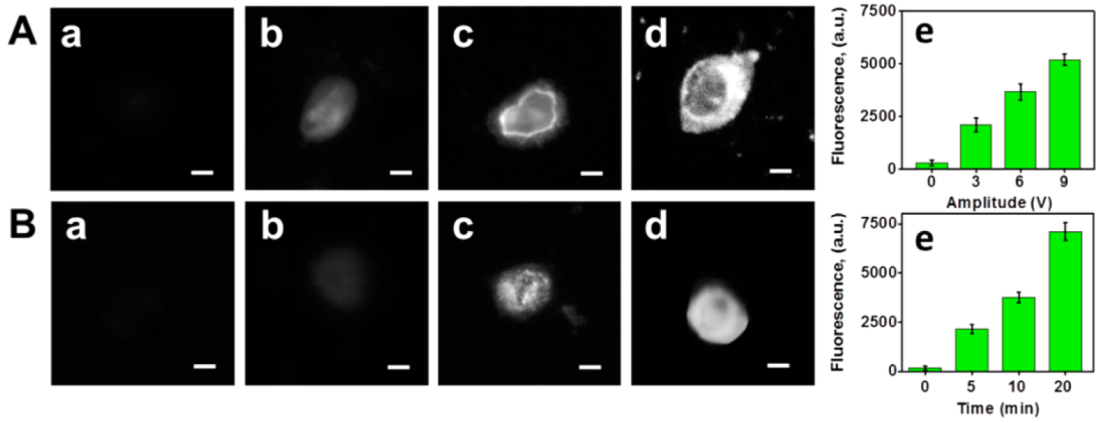

Figure 6. Recovery of the fluorescence in intact MCF-7 cells due to the hybridization process between the immobilized ssDNA (onto the AuNWs) and the endogenous target miRNA-21 overexpressed into these metastatic breast cells. (A) Fluorescence images of the MCF-7 cells after 10 min incubation with the modified AuNWs using (a) static conditions, and under US field (2.66 MHz) at different voltages: 3 V (b), 6 V (c), and 9 V (d). (e) Dependence of the fluorescent signal upon the voltage amplitude. (B) Fluorescence images corresponding to the MCF-7 cells (a–d) after incubation with the ssDNA@GO-modified AuNWs using different US propulsion times: 0 (a), 5 (b), 10 (c), and 20 (d) min, at 6 V and 2.66 MHz. (e) Dependence of the fluorescence signal upon the US exposure time. Scale bar, 10 μm. Error bars estimated as a triple of the standard deviation ($n = 3$).

and at room temperature by guiding the ssDNA@GO-functionalized gold nanomotors to the target cell. While the most widely used detection methods require multiple steps and prior total RNA extraction to perform the miRNAs determination, the new concept offers a much simpler, shorter and a nondestructive single-step approach to examine the endogenous miRNA expression in individual target cells, which could be used for further downstream analysis. Moreover, the proposed strategy helps to resolve the main challenge of the few reported works that allow the miRNA detection in intact cells but required higher cell density and longer incubation times.[16] In comparison with these approaches, which were only able to reflect the average expression of the target miRNA across the collected cell population, the developed assay allowed studying miRNA expression at the single-cell level, which enables distinguishing between cells of the same sample type with different expression.

CONCLUSIONS

In summary, we presented for the first time a single-step nanomotor-based strategy for rapid monitoring of miRNA-21 expression in individual intact cancer cells. This new approach is based on measuring the ("OFF-ON") fluorescence signal (GO quenching-dependable) of internalized US-powered ssDNA@GO-functionalized AuNW motors due to the hybridization of the specific FAM-ssDNA probe immobilized onto the motors with the endogenous target miRNA. The presented results demonstrate the feasibility of this methodology to assess the differential endogenous expression of a target miRNA in single intact cells in a few minutes compared to several hours and high number of cells required by existing miRNA detection methods. These major improvements in sensitivity and detection time have been attributed to the faster internalization process of the nanomotors and their rapid movement inside the cells upon applying the US field, which increases the probability of probe–target contacts and results in a faster and more efficient hybridization. The new simple and rapid nanomotor biosensing tool could find important applications for profiling miRNAs expression at the single-cell level in a wide variety of preclinical and clinical scenarios, monitoring the expression of miRNA in living cells essential to elucidate the roles of miRNA during complex regulatory processes and to assess endogenous miRNAs expression in circulating tumor cells. These attractive features make it very promising in cancer diagnostics, patient follow-up and monitoring of metastatic processes. The inclusion of a magnetic segment in the nanomotor structure would enable their guidance by an external magnetic field.

The key advantage of the new nanomotor fluorescent sensing technology is the ability to perform *in situ* single-step target miRNA analysis within a single intact cell using a short time. This unique capability made it an extremely attractive screening methodology, readily translated to *point-of-care* devices, and to the determination of other important endogenous biomarkers, such as siRNAs, piRNAs or proteins merely by using probe-modified nanomotors labeled with different dyes.

EXPERIMENTAL SECTION

Reagents and Solutions. Graphene oxide (GO) dispersion in H_2O (2 mg/mL, ~0.5 μm length by ~0.5 μm thickness and >95% monolayer GO with thickness around 0.8–1.2 nm), cysteamine hydrochloride, *N*-hydroxysuccinimide (NHS), 1-(3-(dimethylamino)propyl)-*N*′-ethylcarbodiimide hydrochloride (EDC),

2-(*N*-morpholino) ethanesulfonic acid (MES), bovine serum albumin (BSA), Tris-HCl, ethylenediamine tetraacetic acid (EDTA), KCl, NaCl, and $MgCl_2$ were purchased from Sigma-Aldrich.

All the used synthetic oligonucleotides were purchased from Integrated DNA Technologies, Inc. (San Diego, CA) and are listed in Supporting Information Table S1. The synthetic oligonucleotides were dissolved in TE buffer prepared in nuclease-free water (10 mM Tris-HCl, pH 8.0, containing 1 mM EDTA), divided into small 100 μM aliquots, and stored at −20 °C until use.

MCF-7 and HeLa cancer cell lines were obtained from the University of California—San Diego (UCSD), Nanomaterials & Nanomedicine Laboratory. Both cell lines were grown onto glass slides placed into Petri dishes containing DMEM (Dulbecco's modified Eagle's medium), supplemented with 10% fetal bovine serum, penicillin and streptomycin, and 2.5 mM L-glutamine (GIBCO-Invitrogen, Carlsbad, CA), and the cells were used immediately for the experiments. To prepare the cells suspension, after removing the cell culture media, cells were detached from the glass slide and resuspended in 20 mM Tris-HCl, pH 7.4, containing 100 mM NaCl, 5 mM KCl, and 5 mM $MgCl_2$.

The following buffer solutions, prepared with Milli-Q water were used: 20 mM Tris-HCl, pH 7.4, containing 100 mM NaCl, 5 mM KCl, and 5 mM $MgCl_2$ for the FAM-labeled ssDNA immobilization onto the GO-functionalized AuNWs, and the hybridization process, and 20 mM Tris-HCl, pH 7.4, containing 100 mM NaCl, 1 mM EDTA, and 100 μg mL^{-1} of BSA to perform all the washing steps.

A 5 μg mL^{-1} GO dispersion prepared in deionized water was used to modify the AuNWs. Activation of the GO-carboxylic groups was carried out using a 400 mM EDC/100 mM NHS mixture solution prepared in 0.1 M MES buffer pH 6.5.

Standard solutions of the oligonucleotides were prepared daily from the 100 μM stored aliquots in 20 mM Tris-HCl, pH 7.4, containing 100 mM NaCl, 5 mM KCl, and 5 mM $MgCl_2$.

All chemicals used were of analytical-grade reagents, and deionized water was obtained from a Millipore Milli-Q purification system (18.2 MΩ cm at 25 °C).

Nanomotors Fabrication. The AuNWs were prepared by a common template-directed electrodeposition protocol. A thin gold film was first sputtered on one side of the porous alumina membrane template containing 200 nm diameter cylindrical nanopores (Catalogue No. 6809−6022; Whatman, Maidstone, U.K.) to serve as a working electrode. The membrane was assembled in a Teflon plating cell with aluminum foil serving as an electrical contact for the subsequent electrodeposition. A sacrificial copper layer was electrodeposited into the branched area of the membrane using a 1 M cupric sulfate pentahydrate solution ($CuSO_4 \cdot 5H_2O$, Sigma-Aldrich, St. Louis, MO), using a charge of 8 C and a potential of −0.90 V (vs a Ag/AgCl reference electrode, along with a Pt-wire as a counter electrode). The removal of this sacrificial layer helps to create the concave shape in one end of the gold wire motor. Subsequently, Au was plated using a commercial gold plating solution (Orotemp 24 RTU RACK; Technic, Inc., Anaheim, CA) at −1 V (vs Ag/AgCl), using a charge of 4 C. The resulting AuNWs had a length of around 4 μm. The sputtered gold layer and the copper sacrificial layer were simultaneously removed by mechanical polishing using cotton tip applicators soaked with 0.5 M $CuCl_2$ solution in 20% HCl. The membrane was then dissolved in a 3 M NaOH solution for 30 min to completely release the nanowires. The resulting nanomotors were separated from solution by centrifugation at 7000 rpm for 5 min and washed repeatedly with ultrapure water (18.2 MΩ cm) until a neutral pH was achieved. Between washing steps, the nanomotors solution was mixed with ultrapure water and briefly sonicated (2−5 s) to ensure complete dispersion of nanomotors in the washing water. All AuNWs were stored in 1 mL of ultrapure water at room temperature.

Nanomotors Modification. The external gold surface of the nanowires was modified by an overnight immersion in a 2 mM cysteamine hydrochloride solution prepared in water, to obtain an appropriate self-assembly monolayer. A mixture solution, consisting of 5 μg mL^{-1} GO water dispersion and 400 mM EDC/100 mM NHS solution prepared in 0.1 M MES buffer (pH 6.5), was allowed to react during 30 min under shaking, in order to activate the GO-carboxylic groups. After washing with ultrapure water (by centrifugation at 7000 rpm for 3 min), the cysteamine-modified AuNWs were incubated with the GO/EDC/NHS mixture solution during 1 h under shaking. After another washing step with ultrapure water, the GO-modified AuNWs were incubated in a 1 μM FAM-labeled ssDNA solution prepared in 20 mM Tris-HCl, pH 7.4, containing 100 mM NaCl, 5 mM KCl, and 5 mM $MgCl_2$, and allowed to react during 45 min under soft shaking. Finally, the FAM-ssDNA@GO-modified AuNWs were washed twice with the washing buffer. All incubation steps were carried out at room temperature.

AuNWs without FAM-labeled ssDNA or GO were also prepared using the same protocol to perform the corresponding control experiments.

***In Vitro* miRNA Detection.** The *in vitro* miRNA-21 detection protocol involved the duplex formation between the FAM-labeled ssDNA released from the AuNWs surface and the miRNA-21 added to the modified-nanowires solution. To perform these experiments, 100 nM of the synthetic target miRNA-21 (prepared in 20 mM Tris-HCl buffer, pH 7.4, containing 100 mM NaCl, 5 mM KCl and 5 mM $MgCl_2$) was added to the GO@ssDNA AuNWs solution, and different incubation times were studied, in static conditions and applying ultrasound (2.66 MHz) at different amplitude voltages. After that, the sample was collected and the fluorescence signal was measured in the microscope. Same protocol was used to evaluate the selectivity toward the mismatched 1-m sequence. All the experiments were carried out at room temperature.

Intracellular miRNA Detection. To determine the endogenous level of target miRNA-21 in intact cancer cells, a mixture of 1.5 μL of the cell suspension (~1.0 × 10^5 cells/mL) and 1.5 μL of the ssDNA@GO-AuNWs was prepared and different US propulsion times and amplitude voltages were studied at 2.66 MHz. After each study, the fluorescence signal of each sample was checked in the microscope.

Videos were captured using Cool SNAP HQ^2 camera, 20× and 40× objectives and acquired at the frame rate of 10 using the Metamorph 7.1 software (Molecular Devices, Sunnyvale, CA). A Nikon Eclipse 80i upright microscope with B2-A FAM filter was used to capture fluorescence images and videos. The fluorescence signal produced by the hybridization process between the ssDNA probe and the target miRNA-21 was estimated by analyzing the corresponding time lapse images using the software ImageJ.

Ultrasound Equipment. The acoustic cell setup consisted of a piezoelectric transducer (Ferroperm PZ26 disk 10 mm diameter, 0.5 mm thickness) responsible for the generation of US waves, attached by conductive epoxy glue to the bottom center of a steel plate (50 mm × 50 mm × 0.94 mm); then the steel plate was covered with a 240 μm kapton tape protective layer and a sample reservoir at the center (5 mm). A glass slide was used to cover the reservoir for US reflection and to protect the sample. The continuous US sine wave was applied *via* a piezoelectric transducer, through an Agilent 15 MHz arbitrary waveform generator, in connection to a homemade power amplifier. The applied continuous sine waveform had a frequency of 2.66 MHz and voltage amplitude, which varied between 3 and 9 V, to modulate the intensity of the acoustic wave.

Conflict of Interest: The authors declare no competing financial interest.

Supporting Information Available: Supporting videos description, supporting figures and supporting table. The Supporting Information is available free of charge on the ACS Publications website at DOI: 10.1021/acsnano.5b02807.

Acknowledgment. This work was supported by the Defense Threat Reduction Agency Joint Science and Technology Office for Chemical and Biological Defense (grants nos. HDTRA1-13-1-0002 and HDTRA1-14-1-0064). A. Martín and F. Soto, acknowledge the FPU fellowship from the Spanish Ministry of Education,

Culture and Sports, and from the UC MEXUS-CONACYT Doctoral Fellow, respectively.

REFERENCES AND NOTES

1. Dong, H.; Lei, J.; Ding, L.; Wen, Y.; Ju, H.; Zhang, X. MicroRNA: Function, Detection, and Bioanalysis. *Chem. Rev.* **2013**, *113*, 6207–6233.
2. Ryoo, S.-R.; Lee, J.; Yeo, J.; Na, H.-K.; Kim, Y.-K.; Jang, H.; Lee, J. H.; Han, S. W.; Lee, Y.; Kim, V. N.; et al. Quantitative and Multiplexed MicroRNA Sensing in Living Cells Based on Peptide Nucleic Acid and Nano Graphene Oxide (PANGO). *ACS Nano* **2013**, *7*, 5882–5891.
3. Yoo, B.; Kavishwar, A.; Ghosh, S. K.; Barteneva, N.; Yigit, M. V.; Moore, A.; Medarova, Z. Detection of MiRNA Expression in Intact Cells Using Activatable Sensor Oligonucleotides. *Chem. Biol.* **2014**, *21*, 199–204.
4. Planell-Saguer, M.; Rodicio, M. C. Detection Methods for MicroRNAs in Clinic Practice. *Clin. Biochem.* **2013**, *46*, 869–878.
5. Li, J.; Tan, S.; Kooger, R.; Zhang, C.; Zhang, Y. MicroRNAs as Novel Biological Targets for Detection and Regulation. *Chem. Soc. Rev.* **2014**, *43*, 506–517.
6. Keshavarz, M.; Behpour, M. Rafiee-pourb Hossain-Ali. Recent Trends in Electrochemical MicroRNA Biosensors for Early Detection of Cancer. *RSC Adv.* **2015**, *5*, 35651–35660.
7. Pall, G. S.; Codony-Servat, C.; Byrne, C. J.; Ritchie, L.; Hamilton, A. Carbodiimide-Mediated Cross-Linking of RNA to Nylon Membranes Improves the Detection of SiRNA, MiRNA and PiRNA by Northern Blot. *Nucleic Acids Res.* **2007**, *35*, 1–9.
8. Liao, X.; Wang, Q.; Ju, H. Simultaneous Sensing of Intracellular MicroRNAs with a Multi-Functionalized Carbon Nitride Nanosheet Probe. *Chem. Commun.* **2014**, *50*, 13604–13607.
9. Li, J.; Yao, B.; Huang, H.; Wang, Z.; Sun, C. H.; Fan, Y.; Chang, Q.; Li, S.; Wang, X.; Xi, J. Real-Time Polymerase Chain Reaction MicroRNA Detection Based on Enzymatic Stem-Loop Probes Ligation. *Anal. Chem.* **2009**, *81*, 5446–5451.
10. Nelson, P. T.; Baldwin, D. A.; Scearce, L. M.; Oberholtzer, J. C.; Tobias, J. W.; Mourelatos, Z. Microarray-Based, High-Throughput Gene Expression Profiling of MicroRNAs. *Nat. Methods* **2004**, *1*, 155–161.
11. Lee, J. M.; Jung, Y. Two-Temperature Hybridization for Microarray Detection of Label-Free MicroRNAs with Attomole Detection and Superior Specificity. *Angew. Chem., Int. Ed.* **2011**, *50*, 12487–12490.
12. Campuzano, S.; Pedrero, M.; Pingarrón, J. M. Electrochemical Genosensor for the Detection of Cancer-Related MiRNAs. *Anal. Bioanal. Chem.* **2014**, *406*, 27–33.
13. Cheng, Y.; Lei, J.; Chen, Y.; Ju, H. Highly Selective Detection of MicroRNA Based on Distance-Dependent Electrochemiluminescence Resonance Energy Transfer between CdTe Nanocrystals and Au Nanoclusters. *Biosens. Bioelectron.* **2014**, *51*, 431–436.
14. Causa, F.; Aliberti, A.; Cusano, A. M.; Battista, E.; Netti, P. A. Supramolecular Spectrally Encoded Microgels with Double Strand Probes for Absolute and Direct MiRNA Fluorescence Detection at High Sensitivity. *J. Am. Chem. Soc.* **2015**, *137*, 1758–1761.
15. Johnson, B. N.; Mutharasan, R. Sample Preparation-Free, Real-Time Detection of MicroRNA in Human Serum Using Piezoelectric Cantilever Biosensors at Attomole Level. *Anal. Chem.* **2012**, *84*, 10426–10436.
16. Wu, Y.; Han, J.; Xue, P.; Xu, R.; Kang, Y. Nano Metal-Organic Framework (NMOF)-Based Strategies for Multiplexed MicroRNA Detection in Solution and Living Cancer Cells. *Nanoscale* **2015**, *22*, 1753–1759.
17. Yang, C.; Dou, B.; Shi, K.; Chai, Y.; Xiang, Y.; Yuan, R. Multiplexed and Amplified Electronic Sensor for the Detection of MicroRNAs from Cancer Cells. *Anal. Chem.* **2014**, *86*, 11913–11918.
18. Lu, Z.; Zhang, L.; Deng, Y.; Li, S.; He, N. Graphene Oxide for Rapid MicroRNA Detection. *Nanoscale* **2012**, *4*, 5840–5842.
19. Rana, M.; Balcioglu, M.; Robertson, N.; Yigit, M. V. Nano-Graphene Oxide as a Novel Platform for Monitoring the Effect of LNA Modification on Nucleic Acid Interactions. *Analyst* **2014**, *139*, 714–720.
20. Wang, W.; Li, S.; Mair, L.; Ahmed, S.; Huang, T. J.; Mallouk, T. E. Acoustic Propulsion of Nanorod Motors inside Living Cells. *Angew. Chem., Int. Ed.* **2014**, *53*, 3201–3204.
21. Campuzano, S.; Kagan, D.; Orozco, J.; Wang, J. Motion-Driven Sensing and Biosensing Using Electrochemically Propelled Nanomotors. *Analyst* **2011**, *136*, 4621–4630.
22. Vilela, D.; Orozco, J.; Cheng, G.; Sattayasamitsathit, S.; Galarnyk, M.; Kan, C.; Wang, J.; Escarpa, A. Multiplexed Immunoassay Based on Micromotors and Microscale Tags. *Lab Chip* **2014**, *14*, 3505–2509.
23. Sanchez, S.; Soler, L.; Katuri, J. Chemically Powered Micro- and Nanomotors. *Angew. Chem., Int. Ed.* **2014**, *54*, 1414–1444.
24. Guix, M.; Mayorga-Martinez, C. C.; Merkoçi, A. Nano/Micromotors in (Bio)chemical Science Applications. *Chem. Rev.* **2014**, *114*, 6285–6322.
25. Wang, J. Self-Propelled Affinity Biosensors: Moving the Receptor Around the Sample. *Biosens. Bioelectron.* **2015**in press.
26. Wang, J. *Nanomachines: Fundamentals and Applications*; Wiley-VCH; Weinheim, Germany, 2013.
27. Paxton, W. F.; Sundararajan, S.; Mallouk, T. E.; Sen, A. Chemical Locomotion. *Angew. Chem., Int. Ed.* **2006**, *45*, 5420–5429.
28. Zhao, G.; Sanchez, S.; Schmidt, O. G.; Pumera, M. Micromotors with Built-in Compasses. *Chem. Commun.* **2012**, *48*, 10090–10092.
29. Zhao, G.; Pumera, M. Magnetotactic Artificial Self-Propelled Nanojets. *Langmuir* **2013**, *29*, 7411–7415.
30. Guix, M.; Orozco, J.; García, M.; Gao, W.; Sattayasamitsathit, S.; Merkoci, A.; Escarpa, A.; Wang, J. Superhydrophobic Alkanethiol-Coated Microsubmarines for Effective Removal of Oil. *ACS Nano* **2012**, *6*, 4445–4451.
31. Orozco, J.; Cheng, G.; Vilela, D.; Sattayasamitsathit, S.; Vazquez-Duhalt, R.; Valdés-Ramirez, G.; Pak, O. S.; Escarpa, A.; Kan, C.; Wang, J. Micromotor-Based High-Yielding Fast Oxidative Detoxification of Chemical Threats. *Angew. Chem., Int. Ed.* **2013**, *125*, 13518–13521.
32. Soler, L.; Magdanz, V.; Fomin, V. M.; Sanchez, S.; Schmidt, O. G. Self-Propelled Micromotors for Cleaning Polluted Water. *ACS Nano* **2013**, *7*, 9611–9620.
33. Gao, W.; Wang, J. The Environmental Impact of Micro/Nanomachines: A Review. *ACS Nano* **2014**, *8*, 3170–3180.
34. Wu, Z.; Wu, Y.; He, W.; Lin, X.; Sun, J.; He, Q. Self-Propelled Polymer-Based Multilayer Nanorockets for Transportation and Drug Release. *Angew. Chem., Int. Ed.* **2013**, *52*, 7000–7003.
35. Gao, W.; Dong, R.; Thamphiwatana, S.; Li, J.; Gao, W.; Zhang, L.; Wang, J. Artificial Micromotors in the Mouse's Stomach: A Step toward *in Vivo* Use of Synthetic Motors. *ACS Nano* **2015**, *9*, 117–123.
36. Qiu, F.; Fujita, S.; Mhanna, R.; Zhang, L.; Simona, B. R.; Nelson, B. J. Magnetic Helical Microswimmers Functionalized with Lipoplexes for Targeted Gene Delivery. *Adv. Funct. Mater.* **2015**, *25*, 1666–1671.
37. Kagan, D.; Campuzano, S.; Balasubramanian, S.; Kuralay, F.; Flechsig, G. U.; Wang, J. Functionalized Micromachines for Selective and Rapid Isolation of Nucleic Acid Targets from Complex Samples. *Nano Lett.* **2011**, *11*, 2083–2087.
38. Campuzano, S.; Orozco, J.; Kagan, D.; Guix, M.; Gao, W.; Sattayasamitsathit, S.; Claussen, J. C.; Merkoçi, A.; Wang, J. Bacterial Isolation by Lectin-Modified Microengines. *Nano Lett.* **2012**, *12*, 396–401.
39. Yu, X.; Li, Y.; Wu, J.; Ju, H. Motor-Based Autonomous Microsensor for Motion and Counting Immunoassay of Cancer Biomarker. *Anal. Chem.* **2014**, *86*, 4501–4507.
40. Morales-Narváez, E.; Guix, M.; Medina-Sánchez, M.; Mayorga-Martinez, C. C.; Merkoçi, A. Micromotor Enhanced Microarray Technology for Protein Detection. *Small* **2014**, *10*, 2542–2548.

41. Kagan, D.; Benchimol, M. J.; Claussen, J. C.; Erdene, E.-C.; Esener, S.; Wang, J. Acoustic Droplet Vaporization and Propulsion of Perfluorocarbon-Loaded Microbullets for Targeted Tissue Penetration and Deformation. *Angew. Chem., Int. Ed.* **2012**, *124*, 7637–7640.
42. Garcia-Gradilla, V.; Orozco, J.; Sattayasamitsathit, S.; Soto, F.; Kuralay, F.; Pourazary, A.; Katzenberg, A.; Gao, W.; Shen, Y.; Wang, J. Functionalized Ultrasound-Propelled Magnetically Guided Nanomotors: Toward Practical Biomedical Applications. *ACS Nano* **2013**, *7*, 9232–9240.
43. Garcia-Gradilla, V.; Sattayasamitsathit, S.; Soto, F.; Kuralay, F.; Yardimci, C.; Wiitala, D.; Galarnyk, M.; Wang, J. Ultrasound-Propelled Nanoporous Gold Wire for Efficient Drug Loading and Release. *Small* **2014**, *10*, 4154–4159.
44. Satishkumar, B. C.; Brown, L. O.; Gao, Y.; Wang, C. C.; Wang, H. L.; Doorn, S. K. Reversible Fluorescence Quenching in Carbon Nanotubes for Biomolecular Sensing. *Nat. Nanotechnol.* **2007**, *2*, 560–564.
45. Xu, J.; Sahu, S.; Cao, L.; Bunker, C. E.; Peng, G.; Liu, Y.; Fernando, K. A. S.; Wang, P.; Guliants, E. A.; Meziani, M. J.; et al. Efficient Fluorescence Quenching in Carbon Dots by Surface-Doped Metals - Disruption of Excited State Redox Processes and Mechanistic Implications. *Langmuir* **2012**, *28*, 16141–16147.
46. Morales-Narváez, E.; Pérez-López, B.; Pires, L. B.; Merkoçi, A. Simple Forster Resonance Energy Transfer Evidence for the Ultrahigh Quantum Dot Quenching Efficiency by Graphene Oxide Compared to Other Carbon Structures. *Carbon* **2012**, *50*, 2987–2993.
47. Morales-Narváez, E.; Merkoçi, A. Graphene Oxide as an Optical Biosensing Platform. *Adv. Mater.* **2012**, *24*, 3298–3308.
48. Gao, L.; Lian, C.; Zhou, Y.; Yan, L.; Li, Q.; Zhang, C.; Chen, L.; Chen, K. Graphene Oxide-DNA Based Sensors. *Biosens. Bioelectron.* **2014**, *60*, 22–29.
49. Zhang, M.; Yin, B. c.; Tan, W.; Ye, B. C. A Versatile Graphene-Based Fluorescence "On/Off" Switch for Multiplex Detection of Various Targets. *Biosens. Bioelectron.* **2011**, *26*, 3260–3265.
50. Dong, H.; Zhang, J.; Ju, H.; Lu, H.; Wang, S.; Jin, S.; Hao, K.; Du, H.; Zhang, X. Highly Sensitive Multiple MicroRNA Detection Based on Fluorescence Quenching of Graphene Oxide and Isothermal Strand-Displacement Polymerase Reaction. *Anal. Chem.* **2012**, *84*, 4587–4593.
51. Xu, F.; Shi, H.; He, X.; Wang, K.; Ye, X.; Yan, L.; Wei, S. A Facile Graphene Oxide-Based DNA Polymerase Assay. *Analyst* **2012**, *137*, 3989–3994.
52. Wang, W.; Castro, L. A.; Hoyos, M.; Mallouk, T. E. Autonomous Motion of Metallic Microrods Propelled by Ultrasound. *ACS Nano* **2012**, *6*, 6122–6132.
53. Rao, K. J.; Li, F.; Meng, L.; Zheng, H.; Cai, F.; Wang, W. A Force To Be Reckoned with: A Review of Synthetic Microswimmers Powered by Ultrasound. *Small* **2015**, 10.1002/smll.201403621.
54. Lee, J. U.; Lee, W.; Yoon, S. S.; Kim, J.; Byun, J. H. Site-Selective Immobilization of Gold Nanoparticles on Graphene Sheets and its Electrochemical Properties. *Appl. Surf. Sci.* **2014**, *315*, 73–80.
55. Tu, Y.; Li, W.; Wu, P.; Zhang, H.; Cai, C. Fluorescence Quenching of Graphene Oxide Integrating with the Site-Specific Cleavage of the Endonuclease for Sensitive and Selective MicroRNA Detection. *Anal. Chem.* **2013**, *85*, 2536–2542.
56. Campuzano, S.; Torrente-Rodríguez, R. M.; López-Hernández, E.; Conzuelo, F.; Granados, R.; Sánchez-Puelles, J. M.; Pingarrón, J. M. Magnetobiosensors Based on Viral Protein P19 for MicroRNA Determination in Cancer Cells and Tissues. *Angew. Chem., Int. Ed.* **2014**, *53*, 6168–6171.
57. Iorio, M. V.; Ferracin, M.; Liu, C.-G.; Vernese, A.; Spizzo, R.; Sabbioni, S.; Magri, E.; Pedriali, M.; Fabbri, M.; Campiglio, M.; et al. MicroRNA Gene Expression Deregulation in Human Breast Cancer. *Cancer Res.* **2005**, *65*, 7065–7070.
58. Yan, L. X.; Wu, Q. N.; Zhang, Y.; Li, Y. Y.; Liao, D. Z.; Hou, J. H.; Fu, J.; Zeng, M. S.; Yun, J. P.; Wu, Q. L.; et al. Knockdown of MiR-21 in Human Breast Cancer Cell Lines Inhibits Proliferation, *in Vitro* Migration and *in Vivo* Tumor Growth. *Breast Cancer Res.* **2011**, *13*, R2.
59. Tomaselli, S.; Galeano, F.; Alon, S.; Raho, S.; Galardi, S.; Polito, V. A.; Presutti, C.; Vincenti, S.; Eisenberg, E.; Locatelli, F. Modulation of MicroRNA Editing, Expression and Processing by ADAR2 Deaminase in Glioblastoma. *Genome Biol.* **2015**, *16*, No. 510.1186/s13059-014-0575-z.
60. Bussy, C.; Ali-Boucetta, H.; Kostarelos, K. Safety Considerations for Graphene: Lessons Learnt from Carbon Nanotubes. *Acc. Chem. Res.* **2013**, *46*, 692–701.
61. Honda, S.; Kirino, Y. Dumbbell-PCR: A Method to Quantify Specific Small RNA Variants with a Single Nucleotide Resolution at Terminal Sequences. *Nucleic Acids Res.* **2015**, 10.1093/nar/gkv218.